Intracellular activity of cortical and thalamic neurones during high-voltage rhythmic spike discharge in Long-Evans rats *in vivo*

Pierre-Olivier Polack and Stéphane Charpier

Institut National de la Santé et de la Recherche Médicale U667, Collège de France, Paris F-75231 and Université Pierre et Marie Curie, Paris F-75005, France

Spontaneous high-voltage rhythmic spike (HVRS) discharges at 6–12 Hz have been widely described in the electrocorticogram (EcoG) of Long-Evans rats. These ECoG oscillations have been proposed to reflect a state of attentive immobility allowing the optimization of sensory integration within the corticothalamic pathway. This hypothesis has been challenged by recent studies emphasizing similarities between HVRS discharges and spike-and-wave discharges (SWDs) in well-established rat genetic models of absence epilepsy. Here, we made *in vivo* intracellular recordings to determine, for the first time, the cellular mechanisms responsible for the synchronized oscillations in the corticothalamic loop during HVRS discharges in the Long-Evans rats. We show that HVRS discharges are associated in corticothalamic neurones with rhythmic suprathreshold synaptic depolarizations superimposed on a tonic hyperpolarization, likely due to a process of synaptic disfacilitation. Simultaneously, thalamocortical neurones exhibit a large-amplitude 'croissant'-shaped membrane hyperpolarization with a voltage sensitivity suggesting a potassium-dependent mechanism. This thalamic hyperpolarizing envelope was associated with a membrane oscillation resulting from interactions between excitatory synaptic inputs, a chloride-dependent inhibitory conductance and voltage-gated intrinsic currents. These cortical and thalamic cellular mechanisms underlying HVRS activity in Long-Evans rats are remarkably similar to those previously described in the thalamocortical networks during SWDs. Thus, the present study provides an additional support to the hypothesis that HVRS activity in Long-Evans rats is an absence-like seizure activity.

(Received 28 October 2005; accepted after revision 5 January 2006; first published online 12 January 2006)
Corresponding author S. Charpier: Institut National de la Santé et de la Recherche Médicale U667, Collège de France, 11 place Marcelin Berthelot, 75231 Paris Cedex 05, France. Email: stephane.charpier@college-de-france.fr

Electrical oscillations are a ubiquitous feature of central nervous systems from invertebrates to higher mammalians (Bullock, 1997). Neuronal oscillations, which can be recorded in many different brain regions, are implicated in a number of physiological processes, such as respiration, sleep–wake cycle, sensory integration, motor activity, memorization and cognitive performance (Buzsaki *et al.* 1994; Sauve, 1999; Basar *et al.* 2000; Steriade, 2000; Engel *et al.* 2001; Salenius & Hari, 2003; Ward, 2003). Oscillatory activities in central neural networks can also underlie a number of neurological diseases including epilepsies and diverse forms of movement disorders (Buzsaki *et al.* 1994; Hutchison *et al.* 2004; Timofeev & Steriade, 2004).

Large-scale electrical oscillations have long been recognized in the electrocorticogram (ECoG). Cortical oscillations, which essentially reflect coherent rhythmic activity within the corticothalamic loops, are classically subdivided into different types on the basis of their specific range of frequencies and/or cortical localization, such as θ (2–7 Hz), α (7–13 Hz in visual cortex), β (11–30 Hz), γ (30–80 Hz), and μ (7–12 Hz, sensorimotor) rhythms (Mountcastle, 1998; Steriade, 2000, 2003). Besides these physiological rhythms, partial and generalized epileptic seizures are systematically associated with paroxysmal oscillations in the ECoG, which can be limited to a restricted cortical region or synchronized over wide cortical areas (McCormick & Contreras, 2001; Timofeev & Steriade, 2004).

Spontaneous high-voltage rhythmic spike (HVRS) discharges at 6–12 Hz have been found in the ECoG of Long-Evans rats (Semba *et al.* 1980; Semba & Komisaruk, 1984; Kaplan, 1985; Nicolelis *et al.* 1995; Nicolelis & Fanselow, 2002; Wiest & Nicolelis, 2003; Shaw, 2004; Fontanini & Katz, 2005; Shaw & Liao, 2005). These cortical oscillations, which predominate in frontal (motor) and parietal (somatosensory) cortices (Semba *et al.* 1980;

 DOI: 10.1113/jphysiol.2005.100925

Semba & Komisaruk, 1984; Kaplan, 1985; Nicolelis *et al.* 1995; Shaw, 2004; Shaw & Liao, 2005) are associated with rhythmic discharges of single action potentials or bursts in cortical and thalamic neurones (Semba *et al.* 1980; Nicolelis *et al.* 1995; Fanselow & Nicolelis, 1999, 2002). HVRS activity in the Long-Evans rat is concomitant with a quiet behavioural immobility and often shortly precedes very rhythmic, small-amplitude, whisker twitching at a rate similar to that of corresponding HVRS discharges (Semba *et al.* 1980; Semba & Komisaruk, 1984; Nicolelis *et al.* 1995; Shaw, 2004; Shaw & Liao, 2005).

The functional significance of 6–12 Hz HVRS has been the subject of many physiological and pathological hypotheses (see Shaw, 2004 and Shaw & Liao, 2005 for review). Two irreconcilable hypotheses are currently the matter of intense debate. It is proposed that HVRS activities occur during a behavioural state of attentive immobility and represent a dynamical filter optimized for detecting weak and novel tactile stimuli (Fanselow *et al.* 2001; Nicolelis & Fanselow, 2002; Wiest & Nicolelis, 2003). This hypothesis is mainly supported by a recent study suggesting that during periods of HVRS discharges, Long-Evans rats can detect and respond rapidly and reliably to transient whisker deflections (Wiest & Nicolelis, 2003). As a consequence, it is hypothesized (Nicolelis & Fanselow, 2002) that 6–12 Hz HVRS in Long-Evans rats could represent a rodent analogue of the physiological human μ-rhythm and the sensorimotor rhythm of cats, both being also known to occur in a quiet, motionless state (Gastaut, 1952; Kaplan, 1979; Pfurtscheller & Neuper, 1992; Niedermeyer, 1999). The assumption that HVRS activities in Long-Evans rats reflect a normal, non-pathological oscillatory state has been challenged by recent investigations (Shaw, 2004; Shaw & Liao, 2005) emphasizing important similarities between Long-Evans rats and well-established genetic models of the absence epilepsy such as the Genetic Absence Epilepsy Rats from Strasbourg (GAERS, Marescaux *et al.* 1992; Danober *et al.* 1998) and WAG/Rij rats (Coenen *et al.* 1991; Snead *et al.* 1999). In particular, GAERS and WAG/Rij rats exhibit sudden arrests of behaviour often coincident with facial twitching and systematically associated with bilateral and synchronized 7–9 Hz spike-and-wave discharges (SWDs) in the ECoG over wide cortical regions. Moreover, the occurrence of both HVRS discharges in Long-Evans rats and SWDs in GAERS and WAG/Rij rats is dramatically reduced following administration of ethosuximide, a first choice anti-absence drug (Coenen *et al.* 1991; Danober *et al.* 1998; Snead *et al.* 1999; Shaw, 2004).

The aim of the present study was to determine the cellular mechanisms responsible for the synchronized oscillations in the corticothalamic loop during HVRS discharges in the Long-Evans rats. By the means of *in vivo* intracellular recordings, we provide the first description of the synaptic and intrinsic events in cortical and thalamic neurones associated with the spontaneous HVRS discharges occurring in the corresponding ECoG. Our results demonstrate considerable similarities between the cortical and thalamic mechanisms underlying the HVRS activity in Long-Evans rats and the SWDs in GAERS. Thus, they provide an additional support for the hypothesis that spontaneous HVRS in Long-Evans rats is an absence-like seizure activity.

Methods

All experiments were performed in accordance with local Ethical Committee and European Union guidelines (directive 86/609/EEC), and every precaution was taken to minimize stress and the number of animals used in each series of experiments.

Animal preparation

Experiments were performed *in vivo* on 21 adult (10–21 weeks old) female rats from the Long-Evans outbreed. Animals were initially anaesthetized with sodium pentobarbital (40 mg kg^{-1}, I.P.; Sanofi, Libourne, France) and ketamine (100 mg kg^{-1}, I.M.; Imalgène, Merial, France). A cannula was inserted into the trachea, and the animal was placed in a stereotaxic frame. Wounds and pressure points were repeatedly (every 2 h) infiltrated with lidocaine (2%). Once the surgical procedures had been completed (see below), rats were analgesied and maintained in a narcotized and sedated state by injections of fentanyl (3 μg kg^{-1}, I.P.; Janssen-Cilag, Issy-les-Moulinaux, France) repeated every 20–30 min (Simons & Carvell, 1989; Pinault *et al.* 1998; Charpier *et al.* 1999; Slaght *et al.* 2002*a*; Bruno *et al.* 2003; Slaght *et al.* 2004). To obtain long-lasting stable intracellular recordings, rats were immobilized with gallamine triethiodide (40 mg, I.M., every 2 h; Specia, Paris, France) and artificially ventilated. The degree of anaesthesia was assessed by continuously monitoring the ECoG and heart rate, and additional doses of fentanyl were administrated at the slightest change toward an awake pattern (i.e. an increase in the frequency and reduction in amplitude of the ECoG waves and/or an increase in the heart rate). Body temperature was maintained (36.5–37.5°C) with a homeothermic blanket. At the end of the experiments, animals received an overdose of sodium pentobarbital (200 mg kg^{-1}, I.P.).

Electrophysiological recordings

ECoG recordings were obtained with a low impedance (~60 kΩ) silver electrode placed on the dura above the orofacial motor cortex (12 mm anterior to the interaural line; 3.5–4 mm lateral to the midline) (Neafsey *et al.* 1986),

and the reference electrode was placed in a contralateral head muscle.

Intracellular recordings were performed using glass micropipettes filled with 2 M potassium acetate (50–70 MΩ) or 3 M potassium chloride (30–40 MΩ). For intracellular labelling of recorded neurones, 1% neurobiotin (Vector Laboratories, Burlingame, CA, USA) was added to the pipette solution. Measurements of apparent membrane input resistance and time constant were based on the linear electrical cable theory applied to an idealized isopotential neurone (Rall, 1969). Apparent membrane input resistance was assessed by measurement of the mean ($n \geq 10$) membrane potential change at the end of hyperpolarizing current pulses of –0.4 nA (100–200 ms duration, applied every 1.25 s), and the membrane time constant was the time taken for the membrane potential to reach 63% of its final value. When a voltage–current (V–I) relationship, using a wide range of current intensities, could be performed, the membrane input resistance was assessed from the linear portion of the V–I relationship (see Figs 2*D* and 5*Ac*).

Average membrane potentials for cortical and thalamic neurones were determined during inter-HVRS activity, from continuous intracellular records of at least 8 s. When a tip potential was recorded after termination of the intracellular recording, the membrane potential values were corrected accordingly.

Cortical cells, located within the orofacial motor cortex, were recorded within 400 μm of the ECoG electrode at the following coordinates: 12 mm anterior to the interaural line, 3.6–3.8 mm lateral to the midline, and 0.9–2 mm under the cortical surface.

Intracellular recordings of thalamic relay neurones were obtained from the region of the ipsilateral ventrolateral (VL) nucleus in register with the orofacial motor cortex (Rouiller & Welker, 2000). The corresponding stereotaxic coordinates were as follows: 6.2 mm anterior to the interaural line, 1.5 mm lateral to the midline, and 5.5–6.6 mm ventral to the brain surface. The existence of anatomical connectivity between recorded cortical and thalamic regions was confirmed by the antidromic activation of VL neurones after electrical stimulation of the ispilateral orofacial motor cortex. Cortical stimuli used to test antidromic activation (200 μs duration; 10–25 V) were applied with a bipolar concentric electrode (NE-100; Rhodes Medical Instruments, Woodland Hills, CA, USA). The criteria used for identification of antidromic action potentials were as follows: (1) the constant latency of the antidromic response despite imposed changes of membrane potential, (2) collision of the antidromic spikes with spontaneously occurring orthodromic action potentials, and (3) the all-or-none property of the evoked spikes when the stimulation was just below threshold for antidromic activation (see Fig. 5*B*).

Morphological identification

Some intracellularly recorded neurones were labelled using 1% neurobiotin added to the intracellular recording solution. At 1–2 h after the injection, the animal received a lethal dose of pentobarbital and was perfused via the ascending aorta with 500 ml of a physiological solution followed by 500 ml of 0.3% glutaraldehyde and 4% paraformaldehyde in phosphate buffer (PB), 0.1 M, pH 7.4. Brains were postfixed for 2 h in the same fixative solution without glutaraldehyde and then immersed in 30% sucrose PB at 4°C until sectioning. Frozen sections of fixed brains were cut at 50–70 μm in the frontal plane (thalamic neurones) or transversal plane (cortical neurones) and serially collected in PB. After several rinses in PB, neurobiotin was revealed by incubation of the sections in the avidin–biotin peroxidase complex (1 : 100; Vector Laboratories) in PB containing 0.3% Triton X-100 for at least 12 h at 4°C. Incubated sections where washed in PB (two times for 10 min) before immersion in a solution containing 0.005% 3,3′-diaminobenzidine tetrahydrochloride (Sigma, St Louis, MO, USA), 0.4% nickel-ammonium sulphate, and 0.0006% H_2O_2. After several washes in PB, sections were mounted on gelatin-coated slides, counterstained with safarin, and dehydrated through alcohol to xylene for light microscopic examination. The location of labelled neurones within the VL thalamic nucleus or the orofacial motor cortex was confirmed using the atlases of Paxinos & Watson (1986) and Zilles (1985).

Data acquisition and analysis

Intracellular recordings were obtained under current-clamp conditions using the active bridge mode of an Axoclamp-2B amplifier (Axon Instruments, Union City, CA, USA). Data were stored on-line on a DRA 800 digital tape recorder (Biologic, Claix, France) and then digitized with a sampling rate of 10 kHz (intracellular signal), or 1 kHz (ECoG) for off-line analysis. The start and end of a HVRS discharge in the ECoG were taken to be the first and last spike complexes, respectively, where the size of the spike was at least two times the peak-to-peak amplitude of the baseline ECoG. To perform spectral analysis of ECoG potentials, fast Fourier transforms were applied using Spike2 software (Cambridge Electronic Design, Cambridge, UK). The amplitude of action potentials was calculated as the potential difference between their voltage threshold, measured as the membrane potential at which the dV/dt exceeded 10 V s^{-1} (Fricker *et al.* 1999; Mahon *et al.* 2003), and the peak of the spike waveform. Numerical values are given as means ± S.D.

Statistical significance was assessed by performing appropriate statistical tests, one-way ANOVA, Kruskal–Wallis one way analysis of variance on ranks and Dunn's

method. In some measurements a Gauss-Laplace fit was performed. Statistical analysis and curve fitting were performed with Origin 6.0 (OriginLab Corp., Northampton, MA, USA) and SigmaStat 3.0 (SPSS Inc., Chicago, IL, USA).

Results

ECoG properties

Continuous long-lasting (62 ± 43 min) ECoG recordings were obtained from the orofacial motor cortex of Long-Evans rats ($n = 21$) under fentanyl anaesthesia. All recorded animals displayed spontaneous recurrent episodes of HVRS activity (Fig. 1*A*), which usually exhibited a waxing-and-waning pattern (Fig. 1*A* and *B*). HVRS discharges were characterized by a succession of large-amplitude (0.1–1.5 mV) spikes of negative polarity (Fig. 1*A* and *B*). The spike components within the HVRS discharge were often immediately followed by a slow, wave-like, positive ECoG potential (Fig. 1*B* inset). HVRS discharges ($n = 1797$) had a duration of 2.8 ± 2.1 s (from 1 to 39.4 s) (Fig. 1*A*) and the interval between their occurrence was highly variable (32 ± 65 s). The optimal intra-HVRS frequency, revealed by spectral analysis of the ECoG signal, ranged from 6 to 9.5 Hz (7.6 ± 0.8 Hz) (Fig. 1*C*). HVRS discharges spontaneously occurred from a low-amplitude, apparently desynchronized, background ECoG activity (Fig. 1*B* and *C*).

The temporal and morphological properties of HVRS discharges described here, as well as the shape and amplitude of their individual spike components, are consistent with those previously described in freely moving Long-Evans rats (Semba *et al.* 1980; Semba & Komisaruk, 1984; Kaplan, 1985; Nicolelis *et al.* 1995; Shaw, 2004; Shaw & Liao, 2005).

Intrinsic membrane properties of Long-Evans rats cortical neurones

To determine the cortical cellular correlates of HVRS discharges, we performed intracellular recordings of cortical neurones ($n = 18$ cells from 10 Long-Evans rats) located in the orofacial motor cortex simultaneously with the corresponding ECoG. The depth of intracellular recordings, between 900 and 2000 μm from the cortical surface (1460 ± 340 μm, $n = 18$ cells), suggested that the recorded neurones were exclusively located in layer V. This was confirmed by subsequent histological analysis of intracellular labelled neurones ($n = 3$; Fig. 2*A* left), which exhibited the typical morphological features of pyramidal neurones (Feldman, 1984), including a triangular cell body, a prominent apical dendrite extending vertically

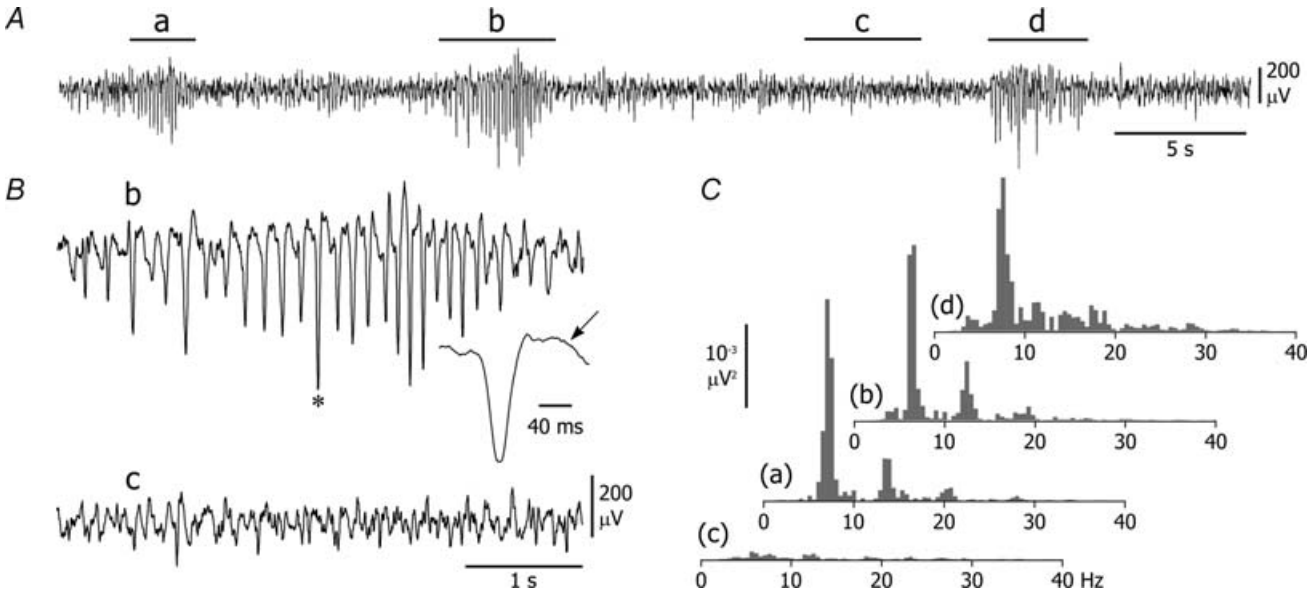

Figure 1. Properties of ECoG activity in Long-Evans rats under fentanyl anaesthesia
A, long lasting (45 s) ECoG recording from the orofacial motor cortex showing the spontaneous occurrence of three HVRS discharges (a, b and d). *B*, expansion of the ECoG segments as indicated by the letters in *A*. The HVRS discharge (b) was composed by a cluster of large-amplitude (> 200 μV) negative spikes. The enlargement of the ECoG spike (inset), marked by the asterisk, shows that the spike component was associated with a slower, wave-like, potential (arrow). *C*, power spectra of the four ECoG epochs as indicated by the letters in *A*. HVRS discharges exhibited a peak frequency with a high-magnitude at 7 Hz (a), 6.6 Hz (b) and 7.6 Hz (d) whereas the spectral analysis of the inter-HVRS activity showed a weak magnitude for the low frequencies (c).

toward the pial surface and basal dendrites radiating out from the base of the soma (Fig. 2*A* right).

The passive electrical membrane properties of cortical neurones, measured during inter-HVRS periods, included a membrane potential of -61 ± 5.2 mV (from -73.5 to -51.2 mV, $n = 18$ cells) (Figs 2*B*, 3*Aa* and 4), an apparent input resistance (Fig. 2*C* and *D*) of 18.2 ± 6.4 MΩ (from 6.3 to 33.6 MΩ, $n = 16$ cells) and a membrane time constant (Fig. 2*C*) ranging between 4 and 25.3 ms (11.9 ± 5.6 ms, $n = 15$ cells). Action potential amplitude ranged between 52 and 74 mV (66 ± 7 mV, $n = 18$ cells) with a total duration of 1.8 ± 0.3 ms ($n = 18$ cells) and a voltage threshold of -51.4 ± 4.1 mV (from -57.2 to -44.1 mV). Each cell displayed a distinctive current-induced firing pattern: either regular-spiking (Fig. 2*B* bottom, $n = 13$ cells) or intrinsically bursting ($n = 5$ cells). However, 5 out 18 cortical cells could exhibit both firing profiles during repetitive direct stimulations (Fig. 2*B*). This observation is consistent with the recent demonstration that neocortical neurone firing pattern may vary in a state-dependent fashion (Steriade, 2004). In some neurones (7 of 18), large-amplitude

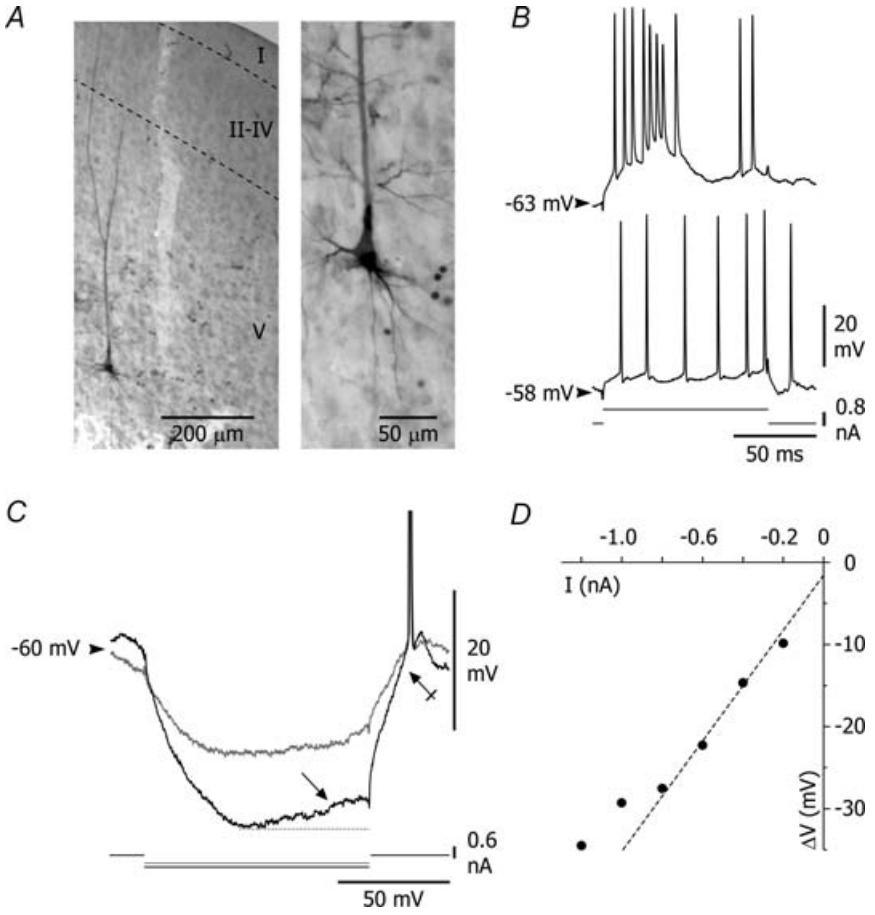

Figure 2. Morphological and electrophysiological properties of Long-Evans rat cortical neurones
A, microphotographs of a neurobiotin-injected cortical pyramidal neurone. The cell had a soma located in the layer V of the orofacial motor cortex and bifurcated apical dendrite projecting to the superficial cortical layers (left). The enlarged view of the somatodendritic region (right) shows that the cell exhibited the typical features of pyramidal cortical neurones including a triangular perikaryon, a thick primary apical dendrite and multiple thin basal dendrites. The axon of this neurone could be followed up to the ventrolateral thalamic nucleus (not shown). *B*, responses (top traces) of the cortical pyramidal cell shown in *A* to two consecutive intracellular injections of the same positive current pulse (lower traces). The cell could display alternatively an intrinsic bursting (upper trace) and regular (bottom trace) pattern. *C–D*, voltage–current relationship. *C*, voltage responses (top traces) of another cortical neurone to negative current pulses of increasing intensities (bottom traces). Note the presence of a sag potential (arrow) and of a postinhibitory rebound of depolarization (crossed arrow) induced by the –0.8 nA current pulse. *D*, plot of the mean ($n = 10$) voltage changes (ΔV) as a function of the current intensity (I). Each data point was calculated as the voltage deflection measured at the time indicated by the black dot in *C*. The apparent input resistance of this cell (34 MΩ) was calculated from the linear segment (dashed line) of the *I–V* curve. Note the rectification of the membrane potential in response to hyperpolarizing currents < –0.8 nA.

hyperpolarizing current pulses induced a depolarizing sag of membrane potential (Fig. 2*C* arrow) likely due to a hyperpolarization-activated inward cationic current (I_h) (Gutnick & Crill, 1995), and a postinhibitory rebound of depolarization (Fig. 2*C* crossed arrow) possibly provoked by the slow kinetics of I_h and/or by a low voltage-activated Ca^{2+} current (I_T) (Gutnick & Crill, 1995).

Intracellular activity of cortical neurones during HVRS discharges

In eight paired cellular and ECoG recordings, we could characterize the intracellular activity of cortical neurones during spontaneous transitions between quiescent ECoG periods and HVRS discharges. During inter-HVRS epochs, the arrhythmic ECoG activity was associated

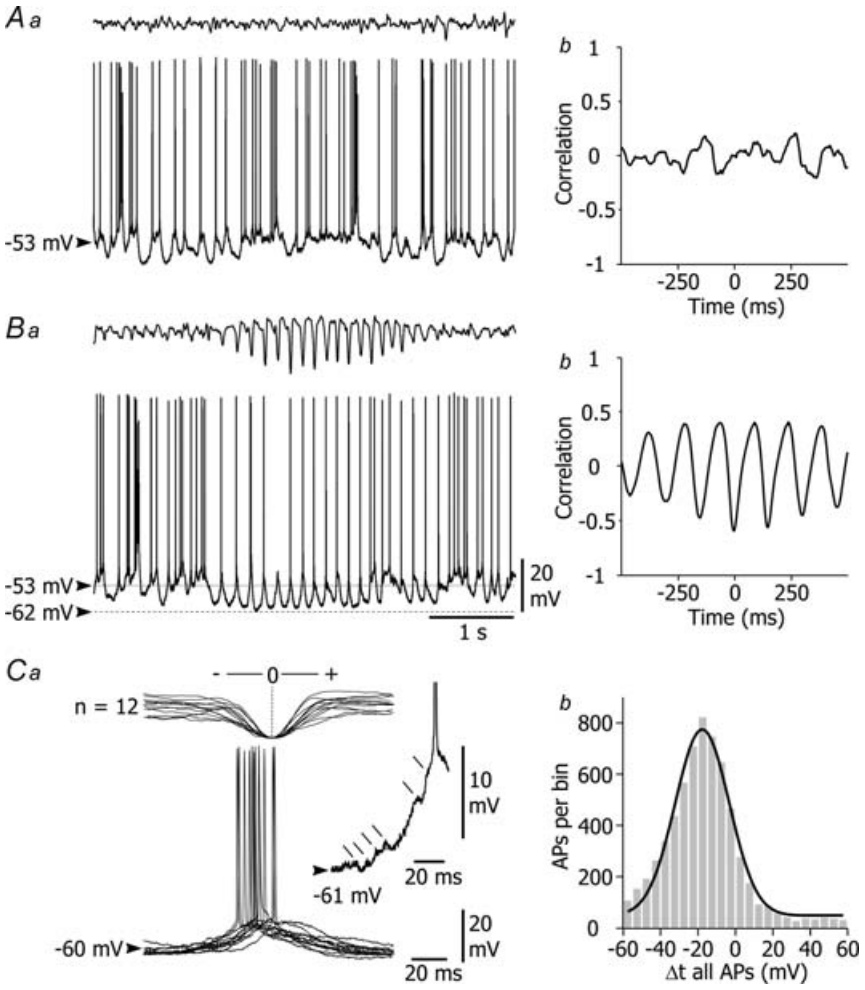

Figure 3. Spontaneous intracellular activity of cortical neurones and its relationship to ECoG waves
A, inter-HVRS activity. *Aa,* irregular membrane potential fluctuations and firing pattern in a pyramidal cortical neurone (bottom trace) during an inter-HVRS ECoG period. *Ab*, the cross-correlogram between the ECoG and intracellular activities indicated a weak temporal coherence between the two signals. *B*, HVRS activity. *Ba*, the occurrence of an HVRS discharge in the ECoG was accompanied in the cortical neurone by rhythmic suprathreshold membrane depolarizations superimposed on a tonic hyperpolarization that lasted for the entire HVRS activity. The continuous line indicates the mean membrane potential of the cell in between the HVRS discharges (−53 mV) and the dashed line the lowest membrane potential reached during the cellular oscillations (−62 mV). *Bb*, ECoG and intracellular oscillations were highly correlated during the HVRS discharge. *C*, temporal relationship between cortical neurones firing and HVRS activity. *Ca*, superimposition ($n = 12$) of suprathreshold depolarizations (bottom) and of the corresponding ECoG potentials (top) using the peak negativity of the ECoG spike component as the time reference (HVRS period shown in *Ba*). As exemplified by the enlarged record (inset) the rising phase of the cellular oscillations was sculpted by the summation of small depolarizing events (oblique lines). *Cb*, pooled histogram (grey bars, bin = 5 ms) and Gauss-Laplace fit (black line, $r^2 = 0.98$) showing the timing (Δt) of all action potentials (APs) ($n = 6589$ APs from 275 HVRS discharges, $n = 8$ cortical cells) to the peak negativity of the ECoG spike (taken as time 0, see *Ca*). Results depicted in *Aa* to *Ca* are from the same cell.

in cortical cells with irregular, depolarizing and hyperpolarizing, membrane potential fluctuations generating an erratic firing pattern (Fig. 3*Aa*). These apparently random discharges, together with the lack of significant correlation between intracellular and ECoG potentials (Fig. 3*Ab*), strongly suggest a temporally disorganized activity of cortical neurones during inter-HVRS periods. The occurrence of a HVRS discharge in the ECoG was accompanied in cortical neurones with suprathreshold oscillatory membrane depolarizations (Fig. 3*Ba*), which were temporally correlated with the surface cortical oscillations (Fig. 3*Bb*). These findings unveil that cortical cells are engaged in a sustained coherent rhythmic activity during epochs of HVRS. The repetitive membrane depolarizations were superimposed on a tonic hyperpolarization of 7.8 ± 2.2 mV in amplitude (from 5.6 to 11.3 mV; $n = 274$ HVRS discharges, from 8 cells) that lasted for the entire HRVS activity (Fig. 3*Ba* dashed line). A careful examination of individual rhythmic depolarizations indicated that they were progressively sculpted by the temporal summation of high-frequency depolarizing potentials (Fig. 3*Ca* inset), presumably of synaptic origin.

To examine the temporal relationship between cortical neurones firing and the corresponding HVRS discharges, we used the peak negativity of the ECoG spike as the zero-time reference (Fig. 3*Ca*). As illustrated by the superimposed records shown in Fig. 3*Ca*, cortical neurones action potentials mostly preceded the peak of the corresponding ECoG spike and the probability of cell firing in association with individual spike components was as high as 0.57 ± 0.28 (from 0.24 to 0.94, $n = 5419$ ECoG spikes from 8 cells). We found that the probability density of firing could be fitted to a Gauss-Laplace function. As shown in Fig. 3*Cb*, the mean value of the pooled distributions was -16.7 ± 22.7 ms ($n = 6589$ action potentials from 275 HVRS discharges, $n = 8$ cells).

The mean firing rate of cortical neurones was not significantly modified by the occurrence of HVRS discharges in the ECoG (inter-HVRS, 6.3 ± 5.7 Hz, HVRS, 6.5 ± 4.8 Hz; $P = 0.78$; $n = 8$ cells). However, as shown in Fig. 4, illustrating the typical changes in the firing pattern during the transitions in the ECoG activity, cortical neurones displayed during HVRS activity a more rhythmic and regular firing profile. This was evidenced by the dramatic decrease in the standard deviation of the pooled interspike intervals (ISIs) in cortical neurones during HVRS periods compared to the inter-HVRS epochs (inter-HVRS, S.D. = 0.34 s, $n = 52366$ ISIs from 8 cells; HVRS, S.D. = 0.18 s, $n = 9052$ ISIs from 8 cells).

Intrinsic membrane properties of Long-Evans rat thalamocortical neurones

We further studied the cellular mechanisms underlying the HVRS discharges in the corticothalamic loop by performing intracellular recordings in the VL nucleus of the thalamus (Fig. 5*Aa* top), which was in register with the recorded cortical region. Neurobiotin-labelled thalamic neurones ($n = 3$) had the classical morphological features of thalamocortical relay neurones (Sawyer *et al.* 1989; Steriade *et al.* 1997), including a fusiform perikaryon and three to seven stout proximal dendrites, which branched to form more slender distal dendrites (Fig. 5*Aa* bottom).

In a first series of experiments, intracellular records ($n = 10$ cells from 7 Long-Evans rats) were made with potassium acetate (KAc)-filled microelectrodes. The mean

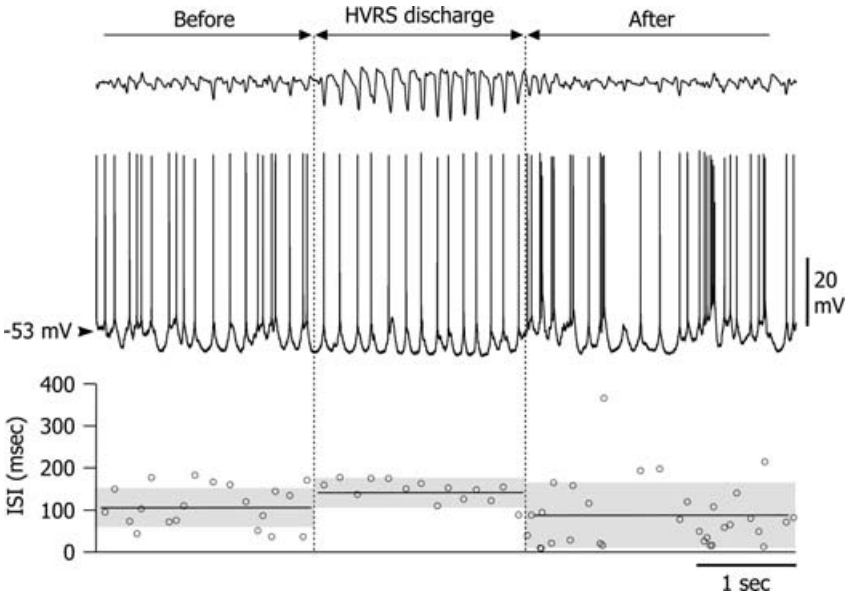

Figure 4. The firing pattern of cortical neurones was modified during the HVRS discharge
Simultaneous recording of the intracellular activity of a cortical neurone (bottom) and of the corresponding ECoG (top). The vertical dashed lines delimit the period of HVRS discharge. The graph below the traces indicates the corresponding values of the intracellular interspike intervals (ISI) before, during and after the HVRS activity. The continuous lines and the width of the grey boxes represent, respectively, the mean and the variances of the interspike intervals (ISIs) for the corresponding 3 recording periods.

membrane potential of thalamocortical neurones during inter-HVRS periods was -57.9 ± 2.9 mV (from -60.9 to -52 mV, $n = 10$) (Figs 5*Ab* and 6*Aa*). The voltage responses to current pulses were used to explore the passive and active membrane properties of thalamocortical neurones. Measurements revealed an apparent input resistance of 22.2 ± 4.4 MΩ (from 14 to 28.3 MΩ, $n = 9$ cells) with a corresponding membrane time constant of 16.4 ± 7 ms (from 8 to 27.7 ms, $n = 9$ cells) (Fig. 5*Ab* and *c*). Action potential amplitude, duration and voltage threshold were 52 ± 5 mV (from 45 to 61, $n = 10$ cells), 1.2 ± 0.1 ms (from 1 to 1.4 ms, $n = 10$ cells) and -53 ± 4 mV (from -56.8 to -45.2 mV, $n = 10$ cells), respectively. In response to suprathreshold current pulses, thalamocortical neurones exhibited a steady train of action potentials (Fig. 5*Ab* and *B* inset) characteristic of the classical tonic firing mode of relatively depolarized thalamocortical neurones (Steriade *et al.* 1997; Sherman, 2001; Destexhe & Sejnowski, 2003).

In all recorded thalamocortical neurones, an examination of *V–I* relationships indicated substantial

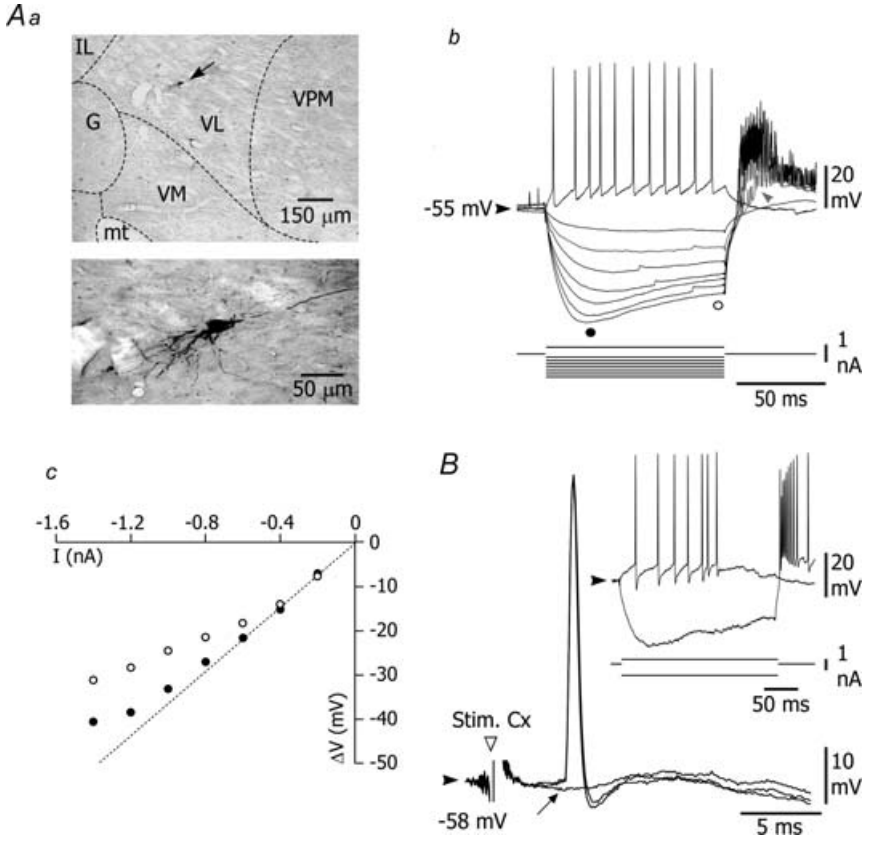

Figure 5. Morphological and electrophysiological properties of Long-Evans rat thalamocortical neurones
Aa, microphotographs of a thalamic neurone labelled by intracellular injection of neurobiotin. Top, the cell (arrow) was localized in the ventrolateral nucleus of the thalamus. G, gelatinosus nucleus; IL, intralaminar nuclei; mt, mammilothalamic tract; VL, ventrolateral thalamic nucleus; VM, ventromedial thalamic nucleus; VPM, ventral posteromedial thalamic nucleus. Bottom, enlarged view of the labelled neurone showing the typical fusiform perikaryon and the numerous varicose dendrites of thalamocortical neurones. *Ab*, voltage responses (top traces) of the thalamic neurone shown in *Aa* to a series of hyperpolarizing and depolarizing current pulses (bottom traces). The traces represent the average of 10 successive trials, except the tonic firing evoked by a single positive current pulse. Note the hyperpolarization-activated depolarizing sag generated by currents greater than –0.8 nA and the postinhibitory rebound, which could be induced (grey arrowhead) in the absence of the sag response (grey trace). *Ac*, corresponding plot of voltage changes (ΔV) as a function of the injected current (I). Measurements were made at the end of membrane capacitance charge (●) and at the end of the pulse (○) as shown in *Ab*. Note the membrane rectification due to the sag potential. The apparent input resistance (24.5 MΩ) was calculated from the linear segment (dotted line) of the *V–I* relationship. *B*, example of thalamocortical neurone identified by its antidromic activation following electrical stimulation of the ipsilateral orofacial motor cortex (open arrow head). As shown by the superimposed ($n = 3$) responses, the activation of the neurone by a threshold stimulus in the absence of an underlying synaptic potential (arrow). Note the fixed antidromic latency (4.3 ms). Inset, voltage responses of the same cell (top traces) to intracellular injection of hyperpolarizing and depolarizing current pulses (bottom traces). Records shown in *A* and *B* are from two different neurones.

non-linearities in the voltage responses to negative current pulses (Fig. 5*Ab* and *c*). This included a hyperpolarization-activated depolarization (Fig. 5*Ab* and *B* inset), likely due to the thalamic mixed cationic conductance (I_h, McCormick & Pape, 1990) and responsible for a strong inward rectification, and a rebound burst firing (Fig. 5*Ab* and *B* inset) on termination of a hyperpolarizing current pulse of sufficient strength, caused by a low-threshold Ca^{2+} potential (LTCP) (Steriade *et al.* 1997; Destexhe & Sejnowski, 2003). The functional connectivity between the thalamic and the cortical regions recorded here was attested by the antidromic activation of thalamocortical neurones following electrical stimulation of the orofacial motor cortex (Fig. 5*B*).

Intracellular activity of thalamocortical neurones during HVRS discharges

Six intracellular recordings from thalamocortical neurones permitted observations on spontaneous transitions between inter- and HVRS activities. The intracellular activity of thalamic cells during inter-HVRS periods was characterized by a barrage of irregular depolarizations responsible for a variable firing pattern, from single discharges to clusters of action potentials (Fig. 6*Aa*), leading to a mean firing rate of 4.8 ± 3.8 Hz (from 0.1 to 9.8 Hz, $n = 6$ cells). The brisk firing of thalamic neurones associated with cortical desynchronization was invariably generated by an oscillatory-like depolarization sculpted by high-frequency barrage of small-amplitude synaptic depolarizations (Fig. 6*Ab*).

We found a good temporal correlation between the onset of HVRS discharges and the occurrence of 'croissant'-shaped hyperpolarization in thalamocortical neurones. The thalamic hyperpolarization mostly started at the onset of the cortical HVRS pattern, was tonic with a mean amplitude of 13.4 ± 3.2 mV (from 9.4 to 18.2 mV, $n = 6$ cells), significantly larger than measured in cortical neurones ($P = 0.002$), and phasic sub- or suprathreshold depolarizing events were superimposed on it (Figs 6*Ba* and 7*Aa–c*). The subthreshold oscillations were characterized by a smooth and slow (~60 ms duration) depolarizing rising phase followed by a faster (~20 ms duration) decaying component (Fig. 6*Bb*) whereas the suprathreshold depolarizations were systematically composed of temporally summating high-frequency synaptic potentials (Fig. 6*Bb* inset) and a LTCP-like depolarization giving rise to single or multiple action potentials (Fig. 6*Bb*). Interestingly, the mean time intervals between unitary depolarizing synaptic events that led to brisk firing was similar between (4.3 ± 3.2 ms, $n = 1560$ synaptic events) and during (4.2 ± 3.8 ms, $n = 722$ synaptic events) HVRS activities ($P > 0.05$, e.g. Fig. 6*Ab* inset *versus Bb* inset).

As illustrated in Fig. 6*C*, intracellular application of long-lasting hyperpolarizing current pulses during inter-HVRS periods could reproduce the sequence of cellular suprathreshold electrical events observed during the cortical oscillations. In this experiment, the spontaneous occurrence of a cluster of depolarizing synaptic potentials (Fig. 6*C* inset), during the hyperpolarization-induced sag potential, triggered a large LTCP crowned by a burst of sodium action potentials.

In 5 of the 6 recorded thalamocortical neurones, the mean firing rate during cortical desynchronization was of 5.7 ± 3.4 Hz and decreased by 45.9% (32.4–66.2%, $n = 5$ cells) by the appearance of HVRS discharges in the ECoG. In the remaining neurone, the very low firing rate in between HVRS periods (0.09 Hz) was slightly enhanced during HVRS activities (1.75 Hz). Across the population ($n = 6$ thalamocortical neurones), the probability of firing in association with the ECoG spikes was of 0.18 ± 0.08 ($n = 153$ HVRS discharges from 6 cells). To assess the temporal relationship between the firing of thalamic neurones and the surface cortical oscillations, we measured the timing of individual thalamic action potentials relative to the peak negativity of the corresponding spike component in the HVRS discharge. The latencies of all action potentials (from one to 6 action potentials per depolarization cycle) led to a unimodal, Gaussian-like distribution with a mean value of −28.6 ± 19.2 ms ($n = 391$ action potentials from 91 HVRS discharges, $n = 6$ cells, Fig. 6*D*).

We attempted to determine the ionic origin of the 'croissant'-shaped hyperpolarizing envelope observed in thalamocortical neurones during HVRS discharges by measuring its amplitude as a function of the membrane potential ($n = 5$ cells), which was maintained at different levels of polarization by DC injections (Fig. 7*A*). The virtual reversal potential of the envelope, assessed by the linear regression fit of the corresponding voltage–dependency plots (Fig. 7*B*), was of −95 ± 10 mV (from −79–104 mV, $n = 5$ cells, Fig. 7*B*), a value consistent with the equilibrium potential of K^+ in thalamic neurones (Destexhe & Sejnowski, 2001).

To test the possible participation of Cl^--dependent events in the activity of thalamocortical neurones during HVRS discharges, thalamic intracellular recordings ($n = 5$ cells from 4 Long-Evans rats) were performed with KCl-filled electrodes. The location and morphological features of Cl^--loaded neurones ($n = 3$ labelled cells) were identical to those of thalamic cells intracellularly recorded with KAc electrodes (see Fig. 8*Aa versus* Fig. 5*Aa* bottom). Electrical membrane parameters of Cl^- loaded thalamocortical neurones were as follows: membrane potential (–58.5 ± 2.4 mV, from −62.1 to −55.7 mV, $n = 5$ cells), apparent input resistance (13.1 ± 3.2 MΩ, from 10 to 17.5 MΩ, $n = 4$ cells) and time constant (6.9 ± 1.1 ms, from 5.7 to 7.8 ms, $n = 3$ cells), action potential amplitude (58 ± 3 mV, from 55 to 62 mV,

$n = 5$ cells), duration (1 ± 0.1 mV, from 1 to 1.1 mV, $n = 5$ cells) and voltage threshold (-53.2 ± 0.7 mV, from -54.1 to -52.4 mV, $n = 5$ cells). Moreover, the active membrane properties of thalamic neurones, including a tonic firing during direct stimulation from the resting potential, a hyperpolarization-induced sag of membrane potential and postinhibitory rebound burst firing (Fig. 8*Ab*) were not altered by the intracellular injection of Cl^-.

We examined the spontaneous activity of three Cl^--loaded thalamocortical neurones during periods of desynchronized ECoG and HVRS. A thalamic tonic hyperpolarization (4 ± 0.3 mV, from 3.8 to 4.3 mV,

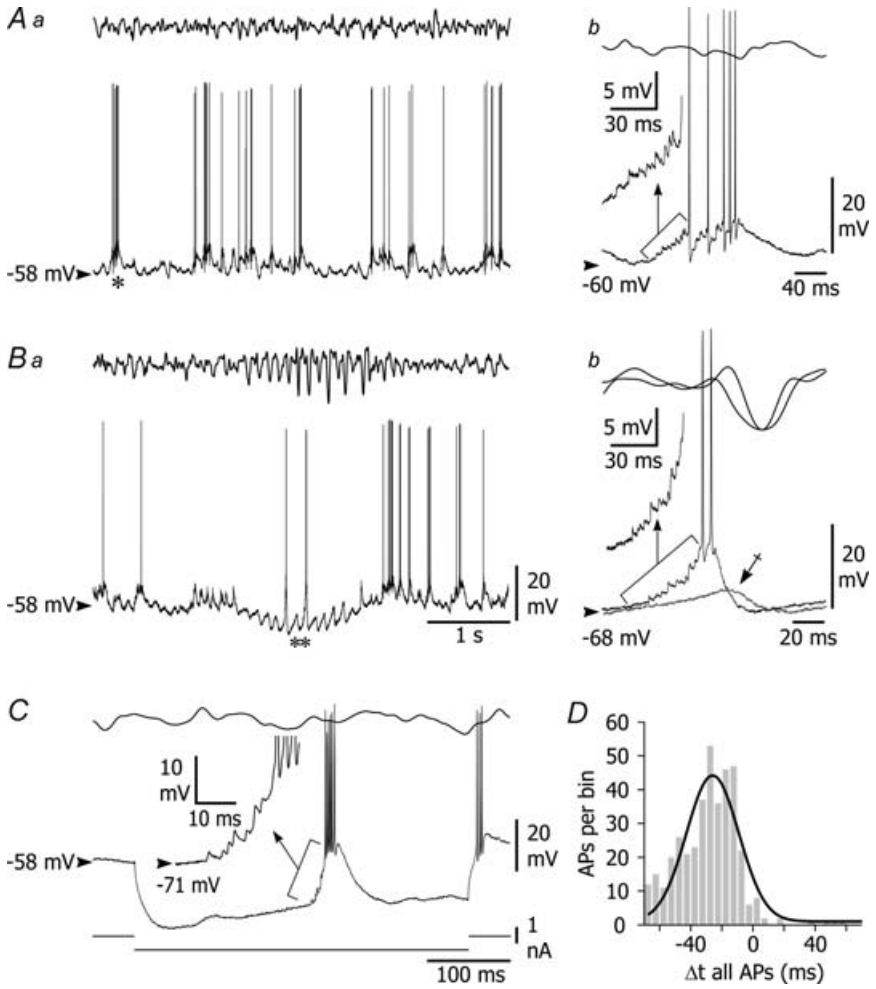

Figure 6. Spontaneous intracellular activity of thalamocortical neurones and its relationship to ECoG waves

A, inter-HVRS activity. *Aa,* spontaneous activity of a thalamocortical neurone (bottom) during an inter-HVRS ECoG period characterized by a sustained depolarizing synaptic activity generating single or clusters of action potentials. *Ab*, expansion of the burst of action potentials (bottom) indicated by the asterisk in *Aa* and of the corresponding ECoG potential (top). The enlarged record (inset) shows that the cluster of action potentials was preceded by high frequency small-amplitude depolarizing events. *B*, HVRS activity. *Ba*, the occurrence of an HVRS discharge in the ECoG (top) was associated in the thalamic neurone (bottom) by rhythmic membrane potential oscillations superimposed on a croissant-shaped hyperpolarization. *Bb*, superimposition of the intracellular suprathreshold and subthreshold (crossed arrow) depolarizations (bottom) indicated by the asterisks in *Ba* and of the corresponding ECoG spikes (top). The expanded record (inset) shows that the suprathreshold depolarization was initiated by the temporal summation of small-amplitude depolarizing potentials. *C*, voltage response (bottom) of a thalamocortical neurone to a long-lasting hyperpolarizing current pulse applied during an inter-HVRS period (top). Note the sag in membrane potential and the spontaneous occurrence of a burst of action potentials generated by a large depolarization driven by the temporal summation of small-amplitude depolarizing potentials (inset). *D*, pooled histogram (grey bars, bin = 5 ms) and Gauss-Laplace distribution (black line, $r^2 = 0.87$) showing the timing (Δt) of all action potentials ($n = 391$ APs from 91 HVRS discharges) in thalamocortical neurones ($n = 6$) with respect to the peak negativity of the ECoG spike (measured as indicated in Fig. 3*Ca*). Records shown in *A–C* are from the same thalamocortical neurone.

$n = 3$ cells) was maintained throughout the HVRS activity (Fig. 8*B* dashed line), indicating that it was not due to a Cl^--dependent conductance. The mean firing rate of these cells was significantly increased by the HVRS activity (inter-HVRS, 6.6 ± 4.8 Hz; HVRS, 12 ± 5.4 Hz, $n = 3$ cells, $P < 0.001$) leading to a robust enhancement in the probability of firing in association with the ECoG spikes (0.51 ± 0.18, $n = 1347$ action potentials from 153 HVRS discharges, Fig. 8*B*). As indicated by the temporal shift in the distribution of firing probability, compared to that of thalamocortical neurones recorded with a KAc-filled electrode (Fig. 8*C*), the increase in firing rate was due to an additional depolarization reflecting a Cl^--dependent conductance largely activated during the decay phase of rhythmic membrane depolarizations (Fig. 8*C* inset).

Discussion

HVRS discharges and spike-and-wave discharges

Cortical HVRS activity recorded from the motor cortex of fentanyl-anaesthetized Long-Evans rats is very similar to that recorded in the freely moving animals (Semba *et al.* 1980; Semba & Komisaruk, 1984; Kaplan, 1985; Wiest & Nicolelis, 2003; Shaw, 2004; Fontanini & Katz, 2005; Shaw & Liao, 2005). In both recording conditions, HVRS discharges occur from a normal background ECoG activity and are characterized by large amplitude, waxing-and-waning, 6–12 Hz oscillations with individual electrical components mostly composed by a fast negative spike followed by a slow positive wave. Moreover, there were no significant differences in the duration or the periodicity of HVRS episodes recorded under fentanyl and during waking (Shaw, 2004). These important findings indicate that our anaesthesia alters neither the processes of initiation of HVRS discharges nor their cellular mechanisms of expression. Thus, it is very likely that the cortical and thalamic intracellular activities described in the present study are identical to those responsible for the HVRS discharges naturally occurring in the freely moving Long-Evans rats.

Recent studies (Shaw, 2004; Shaw & Liao, 2005) pointed out many similarities between the cortical HVRS discharges found in Long-Evans rats and the SWDs spontaneously occurring in genetic models of absence epilepsy, such as GAERS and WGA/Rij rats (Vergnes *et al.* 1982; Drinkenburg *et al.* 1993; Danober *et al.* 1998; Coenen & van Luijtelaar, 2003). HVRS discharges and SWDs exhibit analogous durations and internal frequency, a similar waxing-and-waning pattern with individual electrical events exhibiting the same morphology (Shaw, 2004; present study). In addition, cortical oscillations associated with absence seizures and HVRS activity occur nearly synchronously over widespread cortical areas, except the occipital cortex (Danober *et al.* 1998; Shaw, 2004). The fact that SWDs (Pinault *et al.* 1998; Charpier *et al.* 1999; Slaght *et al.* 2002*a*, 2004; Pinault, 2003; Paz *et al.* 2005) and HVRS discharges (present study) can be recorded under fentanyl, an anaesthesia that precludes the generation of other types of cortical oscillations (Mahon *et al.* 2001), and their blockade by systemic injection of anti-absence medicine (Danober *et al.* 1998; Shaw, 2004), further emphasizes the physiological identity of HVRS and SWD activities.

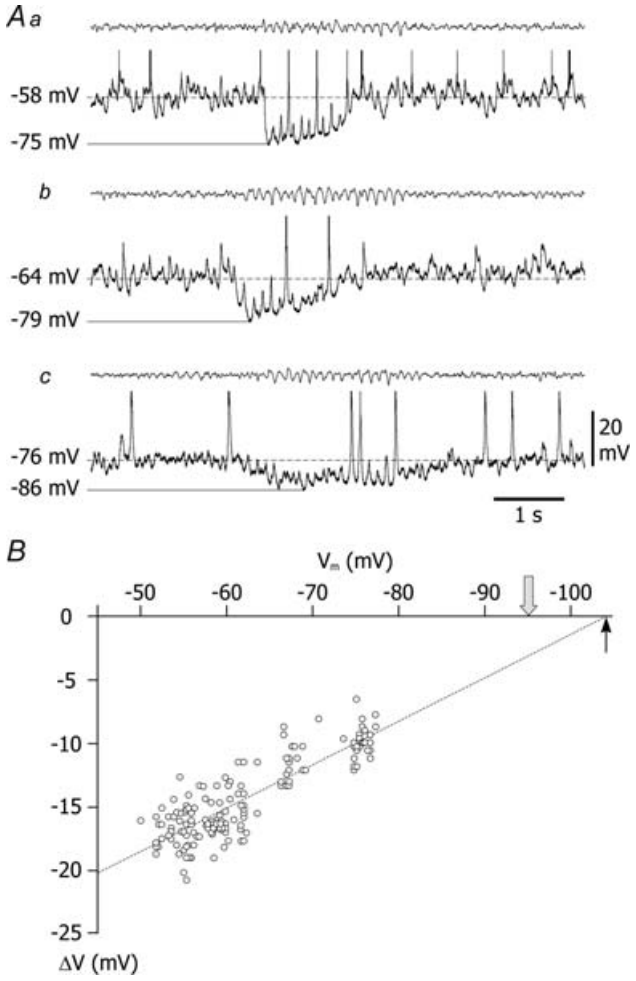

Figure 7. Voltage dependency of the HVRS-associated hyperpolarizing envelope in thalamocortical neurones
A, intracellular activity (bottom traces) of a thalamocortical neurone during HVRS discharges, at rest (*Aa*) and at different levels of membrane potentials achieved by DC injections of −0.5 nA (*Ab*) and −2 nA (*Ac*). The amplitude of the tonic hyperpolarization was measured as the voltage difference between the mean inter-HVRS membrane potential (dashed line) during and the peak hyperpolarization (continuous line) during the cortical oscillations. *B,* corresponding plot ($n = 157$ data points) of the tonic hyperpolarization amplitude (ΔV) as a function of the mean inter-HVRS membrane potential (V_m). The extrapolated reversal potential, estimated from the linear fit (dotted line; $r = 0.86$; $P < 0.0001$) was of −104 mV (arrow). The mean value of the reversal potential (−96 mV) calculated from 5 thalamocortical neurones is indicated by the thick grey arrow.

Cortical mechanisms during HVRS activity

HVRS discharges were associated, in the simultaneously recorded cortical neurones, with rhythmic membrane depolarizations superimposed on a tonic hyperpolarization that lasted for the whole duration of the ECoG oscillations. In theory, the tonic membrane hyperpolarization could result from an active synaptically mediated inhibition or a process of disfacilitation, leading to a passive return to the resting membrane potential due to a transient interruption in the excitatory synaptic inputs to the neurone. The hyperpolarizing shift found in motor cortex pyramidal neurones of Long-Evans rats during HVRS activity is very similar to that described from the same cortical area in GAERS during SWDs (Charpier *et al.* 1999; Slaght *et al.* 2002*b*, 2004; Paz *et al.* 2005). In this case, the seizure-associated membrane hyperpolarization was associated with an increase in membrane input resistance and thus has been attributed to a mechanism of synaptic disfacilitation (Charpier *et al.*

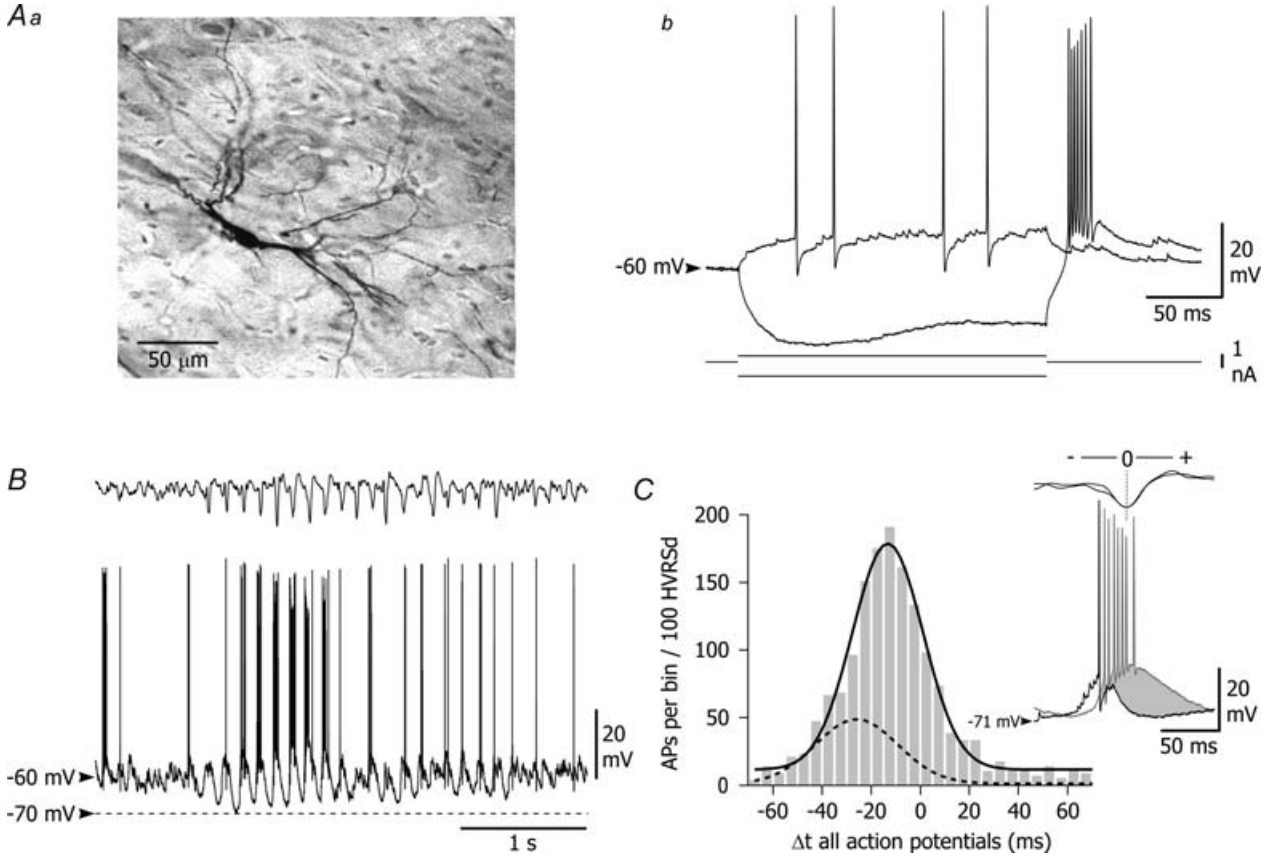

Figure 8. Activity of thalamocortical neurones recorded with KCl-filled microelectrodes
A, morphological and electrophysiological properties of Cl^--loaded thalamocortical neurones. *Aa*, photomicrograph of a thalamocortical neurone labelled by intracellular injection of neurobiotin from the KCl-filled electrode. This neurone, located in the ventrolateral thalamic nucleus, exhibited the typical fusiform perikaryon and numerous varicose dendrites. *Ab*, voltage responses of the thalamocortical cell (top traces) shown in *Aa* to intracellular injection of hyperpolarizing and depolarizing current pulses (bottom traces). Note the tonic firing evoked by the depolarizing current, the hyperpolarization-activated depolarizing sag and the postinhibitory rebound of excitation. *B,* spontaneous intracellular activity of a thalamic neurone recorded with KCl-filled electrodes (bottom trace) simultaneously recorded with the ECoG (top trace). The occurrence of an HVRS discharge was accompanied in the recorded neurone by rhythmic membrane depolarizations crowned by a high-frequency burst of action potentials. Note that the tonic hyperpolarization (dashed line) was still present in this Cl^--loaded neurone. *C*, pooled histogram (grey bars, bin = 5 ms) and Gauss-Laplace distribution (black line, $r^2 = 0.98$) showing the timing (Δt) of all action potentials (APs) in Cl^--loaded thalamocortical cells ($n = 877$ APs from 57 HVRS discharges, $n = 3$ cells) with respect to the peak negativity of the ECoG spike (measured as indicated in the inset). The curve dashed line represents the Gauss-Laplace distribution of action potentials firing in thalamocortical neurones recorded with KAc-filled electrodes (see Fig. 6*D*). To facilitate comparison, the number of action potentials was normalized over 100 HVRS discharges. The inset shows the superimposition of typical suprathreshold cellular depolarizations (bottom) obtained in thalamocortical neurones recorded with KAc- (black record) and KCl-filled microelectrodes (grey record) during ECoG spikes (top). Note the additional membrane depolarization (grey-filled record) and firing in the Cl^--loaded cell.

1999; Slaght *et al.* 2002*b*). A similar process has been also described during cortically generated spike-wave seizures in the cat, where the membrane steady hyperpolarization associated with the ECoG wave component did not result from Cl^--dependent inhibitory potentials (Timofeev *et al.* 2002) but was associated with a significant increase in membrane resistance (Neckelmann *et al.* 2000).

It is very likely that the cortical membrane oscillations associated with the HVRS activity mainly reflect rhythmic synaptic potentials. First, their amplitude is increased during membrane hyperpolarization whereas their frequency is not altered by DC-induced changes in membrane potential (result not shown). These findings, also described in GAERS cortical neurones during SWDs (Charpier *et al.* 1999; Slaght *et al.* 2002*b*, 2004), are consistent with synaptic mechanisms and exclude a significant participation of voltage-gated intrinsic currents. Second, the depolarizing phase of cellular oscillations is sculpted by the temporal summation of high-frequency potentials (Fig. 3*Ca*) exhibiting kinetics and morphological properties compatible with synaptic potentials. These presumed rhythmic synaptic potentials, which occur during the steady hyperpolarization at membrane potentials (< -60 mV) close to or more negative than the equilibrium potential of Cl^-, could reflect a mixture of excitatory glutamatergic synaptic potentials and depolarizing Cl^--dependent GABAergic synaptic events. This hypothesis is consistent with the participation of Cl^--dependent depolarizing postsynaptic potentials in the paroxysmal depolarizing shifts of cortical neurones during ECoG spike-wave activity in cat (Timofeev *et al.* 2002). However, since intracellular current injection reveals a postinhibitory rebound (Fig. 2*C*), possibly due to I_h and/or I_T, we cannot exclude a limited participation of these intrinsic currents in cortical neurones oscillations during HVRS activity.

Because cortical intracellular oscillations are correlated with the spike component of HVRS ECoG activity, and assuming a relatively homogeneous behaviour of cortical neurones during HVRS discharges, our findings indicate that cortical neurones are engaged in a synchronized rhythmic excitation leading to relatively coherent firing (within a ~40 ms temporal window). Such a rhythmic synchrony in cortical cells, which is very similar to that described during SWDs in GAERS (Slaght *et al.* 2004; Paz *et al.* 2005), is consistent with that described from the primary somatosensory and motor cortex of freely moving Long-Evans rats (Nicolelis *et al.* 1995).

Thalamic mechanisms during HVRS activity

We found that HVRS discharges in the ECoG are accompanied in VL thalamic neurones with rhythmic depolarizing events superimposed on a 'croissant'-shaped hyperpolarization. The firing probability of thalamocortical neurones in association with the spike component of the ECoG activity is relatively low (~0.2), and significantly less than that (~0.6) of corticothalamic neurones. This pattern of thalamic intracellular activity and the corresponding firing profile and probability are similar to those already described during SWDs in GAERS (Pinault, 2003) and in the cat VL nucleus during cortical paroxysms (Steriade & Contreras, 1995; Timofeev *et al.* 1998; Timofeev & Steriade, 2004). Moreover, the low firing probability of thalamocortical cells agrees with that calculated during whisker twitching (Fanselow *et al.* 2001) correlated with cortical HVRS discharges in Long-Evans rats (Semba *et al.* 1980; Semba & Komisaruk, 1984; Nicolelis *et al.* 1995; Shaw, 2004; Shaw & Liao, 2005).

We found that the hyperpolarizing envelope in thalamocortical neurones during HVRS activity is virtually abolished around −95 mV. This value may be slightly underestimated due to I_h-induced inward rectification (Pape, 1996) (Fig. 5*Ab* and *c*) that would tend to attenuate the level of membrane polarization reached during the hyperpolarizing envelope. The reversal potential of the envelope (~ -100 mV) is close to the equilibrium potential of K^+, strongly suggesting the implication of postsynaptic K^+-dependent $GABA_B$ receptors. The activation of these receptors, which generates a similar hyperpolarizing envelope in thalamocortical neurones in a pharmacological model of absence seizures *in vitro* (Bal *et al.* 1995), could result from a powerful activation of nucleus reticularis thalami GABAergic neurones, as observed during cortical seizures in cats (Steriade & Contreras, 1995) and GAERS (Slaght *et al.* 2002*a*).

The membrane oscillations in thalamocortical neurones during HVRS are likely to result from complex interactions between synaptic and active intrinsic membrane properties. First, the membrane hyperpolarization, presumably due to the activation of $GABA_B$ receptors, might activate I_h and thus could be responsible for the 'ramp-like' early phase of rhythmic depolarizations. This hypothesis is corroborated by the hyperpolarization-activated sag potential (Fig. 5*Ab* and *c*) indicating the presence of I_h in the recorded thalamocortical neurones. Second, the depolarization achieved by the activation of I_h could suffice to activate I_T, probably deinactivated by the preceding hyperpolarizing envelope, and generate a low-threshold Ca^{2+} spike. This rebound excitation could trigger a single Na^+ action potential or a burst of Na^+ action potentials when the prior depolarization, presumably due to I_h, coincided with a barrage of excitatory synaptic potentials, which probably arose from the rhythmic activity of corticothalamic neurones. This hypothesis is strongly supported by the temporal overlap between the firing distribution of cortical cells (Fig. 3*Cb*) and the occurrence of excitatory synaptic inputs (Fig. 6*Bb*). Third,

intracellular recordings made with a Cl^--filled pipette indicate a powerful Cl^--dependent conductance during the decay phase of the rhythmic membrane depolarizations. This result strongly suggests the implication of $GABA_A$ receptors in the termination of the depolarizing cycle, which could result from the rhythmic bursting of nucleus reticularis thalami GABAergic neurones, as described during cortical seizures in GAERS (Slaght *et al.* 2002*a*). Altogether, this sequence of intracellular events is similar to that recently proposed for the thalamic oscillations during SWDs during absence seizures in GAERS (Pinault, 2003).

Functional significance of HVRS activity in Long-Evans rats

The functional role of 6–12 Hz oscillations in the cortico-thalamic networks of Long-Evans rats is currently the subject of a vivid controversy. A number of behavioural studies, combined with electrophysiological recordings, led to the hypothesis that HVRS discharges provide a normal ECoG rhythm, functionally analogous to the μ-rhythm found in humans and cats (Nicolelis & Fanselow, 2002; Wiest & Nicolelis, 2003). Specifically, these 6–12 Hz oscillations, occurring during 'attentive' and quiet immobility, are suggested to represent a dynamical filter allowing the detection of new and weak sensory stimuli (Nicolelis & Fanselow, 2002; Wiest & Nicolelis, 2003). Such optimized sensory integration in the cortico-thalamic pathway would occur during the membrane hyperpolarization of thalamocortical cells, responsible for a deinactivation of I_T and, consequently, for an increase in neuronal responsiveness (Nicolelis & Fanselow, 2002).

This 'physiological' hypothesis has been recently challenged by many studies describing similarities between HVRS discharges in Long-Evans rats and SWDs associated with absence seizures. First, HVRS discharges are also observed during sleep (Shaw, 2004) and, as we have shown, under fentanyl anaesthesia and thus can occur independently of a behavioural sensorimotor context. Accordingly, these findings also provide an argument against the 'μ-rhythm' hypothesis. Second, the ECoG HVRS activity is very similar to the surface paroxysms seen in well-characterized rat genetic models of absence epilepsy, including cortical spatial distribution, voltage magnitude, and morphological and temporal properties of electrical ECoG events and sensibility to antiabsence drugs (see above). Third, the behavioural correlates of HVRS discharges in Long-Evans rats, characterized by immobility and whisker twitching, are also found in GAERS (Marescaux *et al.* 1992; Danober *et al.* 1998) and WAG/Rij rats (Coenen *et al.* 1991; Snead *et al.* 1999) during SWDs. Moreover, the behavioural arrest and whisker twitching of Long-Evans rats during HVRS periods are analogous to the loss of consciousness and occasional facial twitches associated with human absence seizures (Panayiotopoulos, 1997). Fourth, HVRS discharges are sometimes accompanied by myoclonic jerks (Kaplan, 1985). Fifth, the temporal and spectral profile of HVRS activities is analogous to those of seizure paroxysms induced by penicillin and pentylenetetrazol (Shaw, 2004). Finally, our study, which provides the unique description of the intracellular events underlying HVRS discharges, shows that the neuronal activities in corticothalamic networks during HVRS activity in Long-Evans rats are identical to those described *in vivo* from GAERS and epileptic cats during cortical seizures (see above). These findings, showing the identity of synaptic and membrane mechanisms underlying HVRS discharges and SWDs, strongly suggest that HVRS activity in Long-Evans rats is an absence-like seizure activity.

References

Bal T, von Krosigk M & McCormick DA (1995). Role of the ferret perigeniculate nucleus in the generation of synchronized oscillations *in vitro*. *J Physiol* **483**, 665–685.

Basar E, Basar-Eroglu C, Karakas S & Schurmann M (2000). Brain oscillations in perception and memory. *Int J Psychophysiol* **35**, 95–124.

Bruno RM, Khatri V, Land PW & Simons DJ (2003). Thalamocortical angular tuning domains within individual barrels of rat somatosensory cortex. *J Neurosci* **23**, 9565–9574.

Bullock TH (1997). Signals and signs in the nervous system: the dynamic anatomy of electrical activity is probably information-rich. *Proc Natl Acad Sci U S A* **94**, 1–6.

Buzsaki G, Llinas R, Singer W, Berthoz A & Christen Y (eds) (1994). *Temporal Coding in the Brain*. Springer-Verlag, Berlin, Heidelberg.

Charpier S, Leresche N, Deniau JM, Mahon S, Hughes SW & Crunelli V (1999). On the putative contribution of $GABA_B$ receptors to the electrical events occurring during spontaneous spike and wave discharges. *Neuropharmacology* **38**, 1699–1706.

Coenen AM, Drinkenburg WH, Peeters BW, Vossen JM & van Luijtelaar EL (1991). Absence epilepsy and the level of vigilance in rats of the WAG/Rij strain. *Neurosci Biobehav Rev* **15**, 259–263.

Coenen AM & van Luijtelaar EL (2003). Genetic animal models for absence epilepsy: a review of the WAG/Rij strain of rats. *Behav Genet* **33**, 635–655.

Danober L, Deransart C, Depaulis A, Vergnes M & Marescaux C (1998). Pathophysiological mechanisms of genetic absence epilepsy in the rat. *Prog Neurobiol* **55**, 27–57.

Destexhe A & Sejnowski TJ (2001). *Thalamocortical Assemblies: How Ion Channels, Single Neurons and Large Scale Networks Organize Sleep Oscillations*. Oxford University Press, Oxford.

Destexhe A & Sejnowski TJ (2003). Interactions between membrane conductances underlying thalamocortical slow-wave oscillations. *Physiol Rev* **83**, 1401–1453.

Drinkenburg WH, van Luijtelaar EL, van Schaijk WJ & Coenen AM (1993). Aberrant transients in the EEG of epileptic rats: a spectral analytical approach. *Physiol Behav* **54**, 779–783.

Engel AK, Fries P & Singer W (2001). Dynamic predictions: oscillations and synchrony in top-down processing. *Nat Rev Neurosci* **2**, 704–716.

Fanselow EE & Nicolelis MA (1999). Behavioral modulation of tactile responses in the rat somatosensory system. *J Neurosci* **19**, 7603–7616.

Fanselow EE, Sameshima K, Baccala LA & Nicolelis MA (2001). Thalamic bursting in rats during different awake behavioral states. *Proc Natl Acad Sci U S A* **98**, 15330–15335.

Feldman MD (1984). Morphology of the neocortical pyramidal neuron. In *Cerebral Cortex*, ed. Peters A & Jones EG, pp. 123–200. Plenum Press, New York.

Fontanini A & Katz DB (2005). 7 to 12 Hz activity in rat gustatory cortex reflects disengagement from a fluid self-administration task. *J Neurophysiol* **93**, 2832–2840.

Fricker D, Verheugen JA & Miles R (1999). Cell-attached measurements of the firing threshold of rat hippocampal neurones. *J Physiol* **517**, 791–804.

Gastaut H (1952). Etude électrocorticographique de la réactivité des rythmes rolandiques. *Rev Neurol* **87**, 176–182.

Gutnick MJ & Crill WE (1995). The cortical neuron as an electrophysiological unit. In *The Cortical Neuron*, ed. Gutnick MJ & Mody I, pp. 33–52. Oxford University Press, Oxford.

Hutchison WD, Dostrovsky JO, Walters JR, Courtemanche R, Boraud T, Goldberg J & Brown P (2004). Neuronal oscillations in the basal ganglia and movement disorders: evidence from whole animal and human recordings. *J Neuroscience* **24**, 9240–9243.

Kaplan BJ (1979). Morphological evidence that feline SMR and human mu are analogous rhythms. *Brain Res Bull* **4**, 431–433.

Kaplan BJ (1985). The epileptic nature of rodent electrocortical polyspiking is still unproven. *Exp Neurol* **88**, 425–436.

McCormick DA & Contreras D (2001). On the cellular and network bases of epileptic seizures. *Annu Rev Physiol* **63**, 815–846.

McCormick DA & Pape HC (1990). Properties of a hyperpolarization-activated cation current and its role in rhythmic oscillation in thalamic relay neurones. *J Physiol* **431**, 291–318.

Mahon S, Casassus G, Mulle C & Charpier S (2003). Spike-dependent intrinsic plasticity increases firing probability in rat striatal neurons *in vivo*. *J Physiol* **550**, 947–959.

Mahon S, Deniau JM & Charpier S (2001). Relationship between EEG potentials and intracellular activity of striatal and cortico-striatal neurons: an in vivo study under different anesthetics. *Cereb Cortex* **11**, 360–373.

Marescaux C, Vergnes M & Depaulis A (1992). Neurotransmission in rats' spontaneous generalized nonconvulsive epilepsy. *Epilepsy Res Suppl* **8**, 335–343.

Mountcastle V (1998). *Perceptual Neuroscience: the Cerebral Cortex*. Harvard University Press, Cambridge, MA, USA.

Neafsey EJ, Bold EL, Haas G, Hurley-Gius KM, Quirk G, Sievert CF & Terreberry RR (1986). The organization of the rat motor cortex: a microstimulation mapping study. *Brain Res* **396**, 77–96.

Neckelmann D, Amzica F & Steriade M (2000). Changes in neuronal conductance during different components of cortically generated spike-wave seizures. *Neuroscience* **96**, 475–485.

Nicolelis MA, Baccala LA, Lin RC & Chapin JK (1995). Sensorimotor encoding by synchronous neural ensemble activity at multiple levels of the somatosensory system. *Science* **268**, 1353–1358.

Nicolelis MA & Fanselow EE (2002). Thalamcortical optimization of tactile processing according to behavioral state. *Nat Neurosci* **5**, 517–523.

Niedermeyer E (1999). A concept of consciousness. *Ital J Neurol Sci* **20**, 7–15.

Panayiotopoulos CP (1997). Absence epilepsies. In *Epilepsy, a Comprehensive Textbook*, ed. Engel J & Pedley TA, pp. 2327–2346. Lippincot-Raven, Philadelphia.

Pape HC (1996). Queer current and pacemaker: the hyperpolarization-activated cation current in neurons. *Annu Rev Physiol* **58**, 299–327.

Paxinos G & Watson C (1986). *The Brain in Stereotaxic Coordinates*. Academic Press, Sydney.

Paz JT, Deniau JM & Charpier S (2005). Rhythmic bursting in the cortico-subthalamo-pallidal network during spontaneous genetically determined spike and wave discharges. *J Neurosci* **25**, 2092–2101.

Pfurtscheller G & Neuper C (1992). Simultaneous EEG 10 Hz desynchronization and 40 Hz synchronization during finger movements. *Neuroreport* **3**, 1057–1060.

Pinault D (2003). Cellular interactions in the rat somatosensory thalamocortical system during normal and epileptic 5–9 Hz oscillations. *J Physiol* **552**, 881–905.

Pinault D, Leresche N, Charpier S, Deniau JM, Marescaux C, Vergnes M & Crunelli V (1998). Intracellular recordings in thalamic neurones during spontaneous spike and wave discharges in rats with absence epilepsy. *J Physiol* **509**, 449–456.

Rall W (1969). Time constants and electrotonic length of membrane cylinders and neurons. *Biophys J* **9**, 1483–1508.

Rouiller EM & Welker E (2000). A comparative analysis of the morphology of corticothalamic projections in mammals. *Brain Res Bull* **53**, 727–741.

Salenius S & Hari R (2003). Synchronous cortical oscillatory activity during motor action. *Curr Opin Neurobiol* **13**, 678–684.

Sauve K (1999). Gamma-band synchronous oscillations: recent evidence regarding their functional significance. *Conscious Cogn* **8**, 213–224.

Sawyer SF, Young SJ & Groves PM (1989). Quantitative Golgi study of anatomically identified subdivisions of motor thalamus in the rat. *J Comp Neurol* **286**, 1–27.

Semba K & Komisaruk BR (1984). Neural substrates of two different rhythmical vibrissal movements in the rat. *Neuroscience* **12**, 761–774.

Semba K, Szechtman H & Komisaruk BR (1980). Synchrony among rhythmical facial tremor, neocortical 'alpha' waves, and thalamic non-sensory neuronal bursts in intact awake rats. *Brain Res* **195**, 281–298.

Shaw FZ (2004). Is spontaneous high-voltage rhythmic spike discharge in Long Evans rats an absence-like seizure activity? *J Neurophysiol* **91**, 63–77.

Shaw FZ & Liao YF (2005). Relation between activities of the cortex and vibrissae muscles during high-voltage rhythmic spike discharges in rats. *J Neurophysiol* **93**, 2435–2448.
Sherman SM (2001). Tonic and burst firing: dual modes of thalamocortical relay. *Trends Neurosci* **24**, 122–126.
Simons DJ & Carvell GE (1989). Thalamocortical response transformation in the rat vibrissa/barrel system. *J Neurophysiol* **61**, 311–330.
Slaght SJ, Leresche N, Deniau JM, Crunelli V & Charpier S (2002*a*). Activity of thalamic reticular neurons during spontaneous genetically determined spike and wave discharges. *J Neurosci* **22**, 2323–2334.
Slaght SJ, Paz T, Chavez M, Deniau JM, Mahon S & Charpier S (2004). On the activity of the corticostriatal networks during spike-and-wave discharges in a genetic model of absence epilepsy. *J Neurosci* **24**, 6816–6825.
Slaght SJ, Paz T, Mahon S, Maurice N, Charpier S & Deniau JM (2002*b*). Functional organization of the circuits connecting the cerebral cortex and the basal ganglia: implications for the role of the basal ganglia in epilepsy. *Epileptic Disord* **4** (Suppl. 3), S9–S22.
Snead OC 3rd, Depaulis A, Vergnes M & Marescaux C (1999). Absence epilepsy: advances in experimental animal models. *Adv Neurol* **79**, 253–278.
Steriade M (2000). Corticothalamic resonance, states of vigilance and mentation. *Neuroscience* **101**, 243–276.
Steriade M (2003). *Neuronal Substrates of Sleep and Epilepsy*. Cambridge University Press, Cambridge.
Steriade M (2004). Neocortical cell classes are flexible entities. *Nat Rev Neurosci* **5**, 121–134.
Steriade M & Contreras D (1995). Relations between cortical and thalamic cellular events during transition from sleep patterns to paroxysmal activity. *J Neurosci* **15**, 623–642.
Steriade M, Jones EG & McCormick DA (1997). *Thalamus: Organisation and Function*. Elsevier Science, Oxford.
Timofeev I, Grenier F & Steriade M (1998). Spike-wave complexes and fast components of cortically generated seizures. IV. Paroxysmal fast runs in cortical and thalamic neurons. *J Neurophysiol* **80**, 1495–1513.
Timofeev I, Grenier F & Steriade M (2002). The role of chloride-dependent inhibition and the activity of fast-spiking neurons during cortical spike-wave electrographic seizures. *Neuroscience* **114**, 1115–1132.
Timofeev I & Steriade M (2004). Neocortical seizures: initiation, development and cessation. *Neuroscience* **123**, 299–336.
Vergnes M, Marescaux C, Micheletti G, Reis J, Depaulis A, Rumbach L & Warter JM (1982). Spontaneous paroxysmal electroclinical patterns in rat: a model of generalized non-convulsive epilepsy. *Neurosci Lett* **33**, 97–101.
Ward LM (2003). Synchronous neural oscillations and cognitive processes. *Trends Cogn Sci* **7**, 553–559.
Wiest MC & Nicolelis MA (2003). Behavioral detection of tactile stimuli during 7–12 Hz cortical oscillations in awake rats. *Nat Neurosci* **6**, 913–914.
Zilles K (1985). *The Cortex of the Rat: A Stereotaxic Atlas*. Springer-Verlag, Berlin Heidelberg.

Acknowledgements

This work was supported by the Ecole Nationale Vétérinaire de Nantes and the Institut National de la Santé et de la Recherche Médicale. We thank Dr S. Mahon, Professor J.-M. Deniau and Dr R. Miles for critical discussions on the experiments and thoughtful comments on this manuscript and A.-M. Godeheu for assistance with the histological processing.